Struct Chem (2015) 26:555–563
DOI 10.1007/s11224-014-0512-5

ORIGINAL RESEARCH

Unusual reverse face-to-face stacking in propylene linked pyrazole system: perspective of organic materials

Sunil Kumar Rai · Priyanka Srivastava · Hariom Gupta · Maria del C. Puerta · Pedro Valerga · Ashish Kumar Tewari

Received: 3 June 2014 / Accepted: 4 September 2014 / Published online: 2 October 2014

Abstract Flexible dimers **1**, **2**, and **3** of "pyrazole" derivatives linked with propylene spacer are synthesized and conformational stability in solid, solution, and gaseous states is studied through single crystal X-ray diffraction, 2D NOESY ,and DFT, respectively. The folded conformation of compound **2** is stable in all three states and X-ray diffraction evince that molecule is intramolecularly stacked in reverse face-to-face manner. TEM image of compound **2** exhibits rigid hollow nanospikes with high tendency to form agglomerates.

Keywords 2D NOESY · Density functional theory · Non-covalent interactions · Pyrazole · Single crystal X-ray diffraction · Transmission electron microscopy

Electronic supplementary material The online version of this article (doi:10.1007/s11224-014-0512-5) contains supplementary material, which is available to authorized users.

S. K. Rai · P. Srivastava · A. K. Tewari (✉)
Department of Chemistry (Center of Advanced Studies), Faculty of Science, Banaras Hindu University, Varanasi 221005, India
e-mail: tashish2002@yahoo.com; ashishtewarichem@gmail.com

H. Gupta
Analytical Discipline and Centralized Instrument Facility, CSMCRI, Gijubhai Badheka Marg, Bhavnagar 364021, Gujarat, India

M. del C. Puerta · P. Valerga
Departamento de Ciencia de los, Materiales e Ingenieria Metalurgica, Facultad de Ciencias, Campus Universitario del Rio San Pedro, 11510 Puerto Real, Spain

Introduction

The non-covalent interactions in chemistry, biology, nanotechnology, and crystal engineering play a subtle role in molecular recognition and molecular architecture [1–3]. Weak attractive intramolecular interactions between aromatic rings might play a significant role in determining the preferred conformation of flexible organic molecules [4]. Among various non-covalent interactions, C–H···O, C–H···N, C–H···π ,and π···π have been commonly observed in DNA, RNA, and proteins which control the specific shape and geometry of such large molecules [5–9]. To illustrate the π···π interaction between purine and pyrimidine bases in DNA, Brown et al. [10] used "propylene linker" for the promotion of intramolecular aromatic π···π interaction which was further studied by Leonard , Newcomb, and Gellman [11, 12]. The mystery of how propylene linked aromatic dimers specifies a U-motif has intrigued chemists leading to designing and development of such type of small dimeric foldamers [13, 14]. Various U-motif flexible dimers have been designed to study their properties and useful applications [15–17]. Several molecules have been reported whose conformations in the solid state are stabilized by inter/intramolecular interactions [18–20].

The present study is based on the pyrazole system, which is the better half of pyrazolo[3,4-*d*]pyrimidine [21]. Pyrazolo[3,4-*d*]pyrimidine molecules are well known for their structural diversities [22] but such properties in pyrazole systems [17, 23] have not been documented. Pyrazolone dimers **2** and **3** adopted unusual folded conformation whereas **1** adopted open conformation (Scheme 1). The striking feature of these interesting foldamers was their ability to display U-turn conformations stabilized by intramolecular non-covalent interactions. The intramolecular stacking interactions arose from the interaction

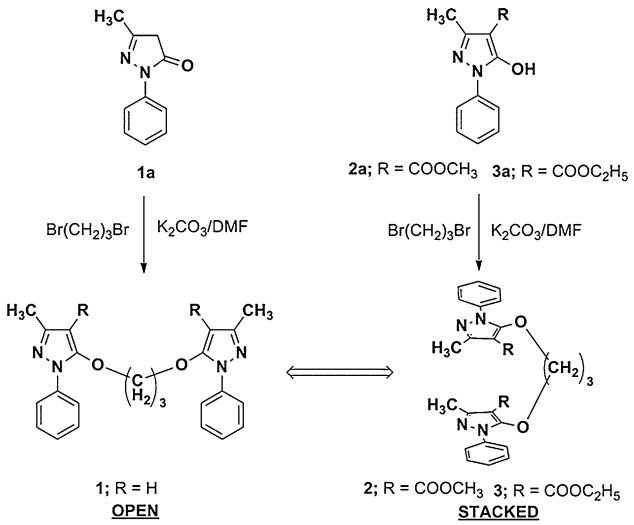

Scheme 1 Synthesis of compounds **1**, **2**, and **3**

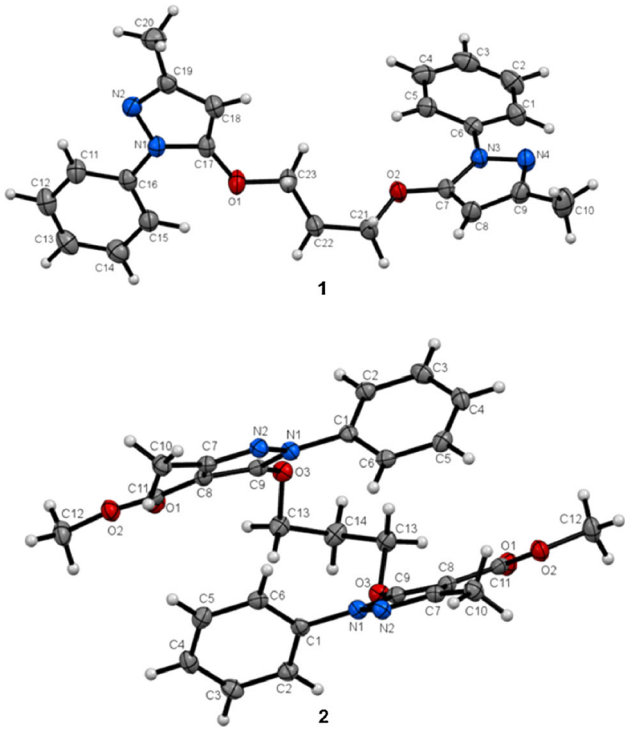

Fig. 1 ORTEP diagram of compounds **1** and **2** (refcode XIMSES), thermal ellipsoids are drawn at 30 and 50 % probability level, respectively

between HOMO of the donor ring and LUMO of the acceptor ring [24]. The length of the spacer was confined to "trimethylene" to promote intramolecular noncovalent interactions. Single crystal X-ray crystallography of pyrazole derivative **1** showed that it existed in open conformation while insertion of an ester group at position 4 of pyrazole ring changed the conformation from open to folded state (Scheme 1 and Fig. 1).

Experimental section

General considerations

^{1}H and ^{13}C NMR spectra were recorded with $CDCl_3$ as the solvent at 300 or 400 MHz spectrometers and TMS as internal standard and chemical shifts have been reported in ppm relative to TMS. All IR spectra values are reported in cm^{-1}. Unless otherwise noted, all reagents were obtained from commercial suppliers and used without further purification.

Synthesis

Compounds **1a**, **2a**, and **3a** were made according to literature procedure [23].

1,3-Bis((3-methyl-1-phenyl-1H-pyrazol-5-yl)oxy) propane (1)

To a stirred solution of compound **1a** (2.00 g, 11.48 mmol) in DMF (10 mL) was added K_2CO_3 (1.59 g, 11.48 mmol) and further stirred for 30 min. Then 1,3-dibromopropane (0.59 mL, 5.74 mmol) was added and stirring was continued for next 20 h. DMF was evaporated at reduced pressure in rotary evaporator and remained solid was extracted in $CHCl_3/H_2O$ mixture. Organic layer was separated and dried over anhydrous Na_2SO_4. After removal of the solvent in vacuo, the crude product was purified by column chromatography (Ethyl acetate/Hexane 1:19) to give compound **1** as white crystalline solids (1.40 g, 62.78 %). Mp. 94–95 °C; ^{1}H NMR (300 MHz, $CDCl_3$, 25 °C, TMS): δ = 7.63 (4H, d, J = 9, *o*-Ph-**H**), 7.40 (4H, t, J = 9, *m*-Ph-**H**), 7.22 (2H, t, J = 9, *p*-Ph-**H**) 5.45 (2H, s, Pyrazole ring-**H**), 4.22 (4H, t, J = 6, O–C**H$_2$**), 2.26 (8H, m, Pyrazole-C**H$_3$** and –C**H$_2$**–); ^{13}C NMR (75 MHz, $CDCl_3$, 25 °C, TMS): δ = 154.2, 148.5, 138.5, 128.6, 125.7, 121.6, 99.1, 86.3, 68.0, 28.4, 14.43; IR (KBr): ν_{max} = 1590, 1559, 1514 cm^{-1}; FAB MS: m/z 389.19 (M+1); elemental analysis calcd (%) for $C_{23}H_{24}N_4O_2$: C 71.11, H 6.23, N 14.42; found: C 71.08, H 6.20, N 14.45.

Dimethyl 5,5'-{propane-1,3-diylbis(oxy)}bis(3-methyl-1-phenyl-1H-pyrazole-4-carboxylate) (2)

Procedure was same as procedure (**1**) but **1a** was replaced by **2a**. Crude product was purified by column chromatography (Ethyl acetate/Hexane 1:9) to give compound **2** as white crystalline solids (50.63 %). Mp. 58–60 °C; ^{1}H NMR (300 MHz, $CDCl_3$, 25 °C, TMS): δ = 7.51 (4H, d, J = 9, *o*-Ph-**H**), 7.39 (4H, t, J = 9, *m*-Ph-**H**), 7.31 (2H, t, J = 9, *p*-Ph-**H**), 4.18 (4H, t, J = 6, O–C**H$_2$**), 3.81 (6H, s, O–C**H$_3$**), 2.45 (6H, s, Pyrazole-C**H$_3$**), 1.99 (2H, quint.,

$J = 6$, –C**H$_2$**–); ^{13}C NMR (75 MHz, $CDCl_3$, 25 °C, TMS): δ = 163.2, 155.0, 150.8, 137.3, 129.1, 128.9, 127.5, 123.2, 99.1, 72.4, 51.0, 30.0, 15.3; IR (KBr): ν_{max} = 1708, 1596, 1550, 1246 cm^{-1}; FAB MS: m/z 505.20 (M+1); elemental analysis calcd (%) for $C_{27}H_{28}N_4O_6$: C 64.27, H 5.59, N 11.10; found: C 64.32, H 5.55, N 11.14.

Diethyl 5,5'-{propane-1,3-diylbis(oxy)}bis(3-methyl-1-phenyl-1H-pyrazole-4-carboxylate) (3)

Procedure was same as procedure (**1**) but **1a** was replaced by **3a**. Crude product was purified by column chromatography (Ethyl acetate/Hexane 1:9) to give compound **3** as white solid below 20 °C (55.50 %). ^{1}H NMR (300 MHz, $CDCl_3$, 25 °C, TMS): δ = 7.51 (4H, d, $J = 9$, *o*-Ph-**H**), 7.38 (4H, t, $J = 9$, *m*-Ph-**H**), 7.30 (2H, t, $J = 9$, *p*-Ph-**H**), 4.31 (4H, q, $J = 6$, O–C**H$_2$**–CH_3), 4.18 (4H, t, $J = 6$, –C**H$_2$**–), 2.46 (6H, s, Pyrazole-C**H$_3$**), 2.01 (2H, quint., $J = 6$, –C**H$_2$**–), 1.37 (6H, t, $J = 6$, O–CH_2–C**H$_3$**); ^{13}C NMR (75 MHz, $CDCl_3$, 25 °C, TMS): δ = 163.0, 154.9, 150.9, 137.3, 129.2, 128.0, 123.5, 99.6, 73.4, 59.9, 32.7, 29.6, 29.2, 15.3, 14.4; IR (KBr): ν_{max} = 1710, 1603, 1551, 1247 cm^{-1}; FAB MS: m/z 533.40 (M+1); elemental analysis calcd (%) for $C_{29}H_{32}N_4O_6$: C 65.40, H 6.06, N 10.52; found: C 65.35, H 5.99, N 10.58.

Crystallization

Compounds **1** and **2** were crystallized by slow evaporation of ethyl acetate at room temperature. Compound **3** formed gel-like mass at room temperature or above 20 °C by slow evaporation of a wide range of solvents or mixture of solvents. Low temperature crystallization of **3** in a light solvent (i.e., acetone) gave white amorphous solids below 0 °C which morphed into gels at room temperature.

X-ray crystallography

Determination of the unit cell and data collection for the compounds were performed with Mo Kα radiation (λ = 0.71073 Å) on a Bruker Smart 1000 diffractometer and equipped with a CCD camera. All of the structures were solved primarily by direct methods and refined with the full-matrix least squares techniques using SHELXS-97 and SHELXL-97 programs [25]. All non-hydrogen atoms were refined with anisotropic thermal parameters. The hydrogen atoms were introduced in calculated positions and refined with a fixed geometry with respect to their carrier atoms. Molecular graphics and ORTEP diagrams (Fig. 1) were designed using Mercury version-3. Crystal data and details of structural determination refinement for compound **1** are summarized in Table 1, while structure information of compound **2** can be obtained from CSD with refcode XIMSES. The selected bond lengths and angles of compound **1** are given in table S1 in the Electronic Supplementary Information.

Table 1 Crystal data and structure refinement parameters for compound **1**

Compound name	1,3-bis((3-methyl-1-phenyl-1H-pyrazol-5-yl)oxy)propane **(1)**
CCDC number	961680
Empirical formula	$C_{23}H_{24}N_4O_2$
Formula weight	388.46
Temperature	100 K
Wavelength	0.71073 Å
Crystal system	Triclinic
Space group	P-1
a	9.143 (2) Å
b	9.2887 (13) Å
c	13.271 (3) Å
α	74.670 (14)°
β	73.209 (19)°
γ	78.841 (15)°
Cell volume	1032.3 (3) Å^3
$D_{calculated}$	1.250 mg/m^3
F(000)	412
Crystal size	0.58 × 0.53 × 0.51 mm
Z	2
R factor (%)	6.10
Theta range	3.3–32.6°
Limiting indices	$-13 \le h \le 13$, $-14 \le k \le 14$, $-20 \le l \le 20$
μ(Mo KR)/mm^{-1}	0.08
R_{int}	0.033
Measured reflexes	11,740
Independent refln	6698
Reflections with $I > 2\sigma(I)$	3255
Parameters	334
Goodness of fit	1.0
$R[F^2 > 2\sigma(F^2)]$	0.061
wR(F^2)	0.161

Results and discussion

Crystallographic evidences

Few examples of trimethylene-linked aromatic/hetero aromatic systems are known to have folded conformation due to intramolecular weak interactions in the solid state [26, 27]. Although excellent crystallographic evidences of C–H···O and C–H···N interactions [28, 29] were first documented by Taylor and Kennard [28] where they

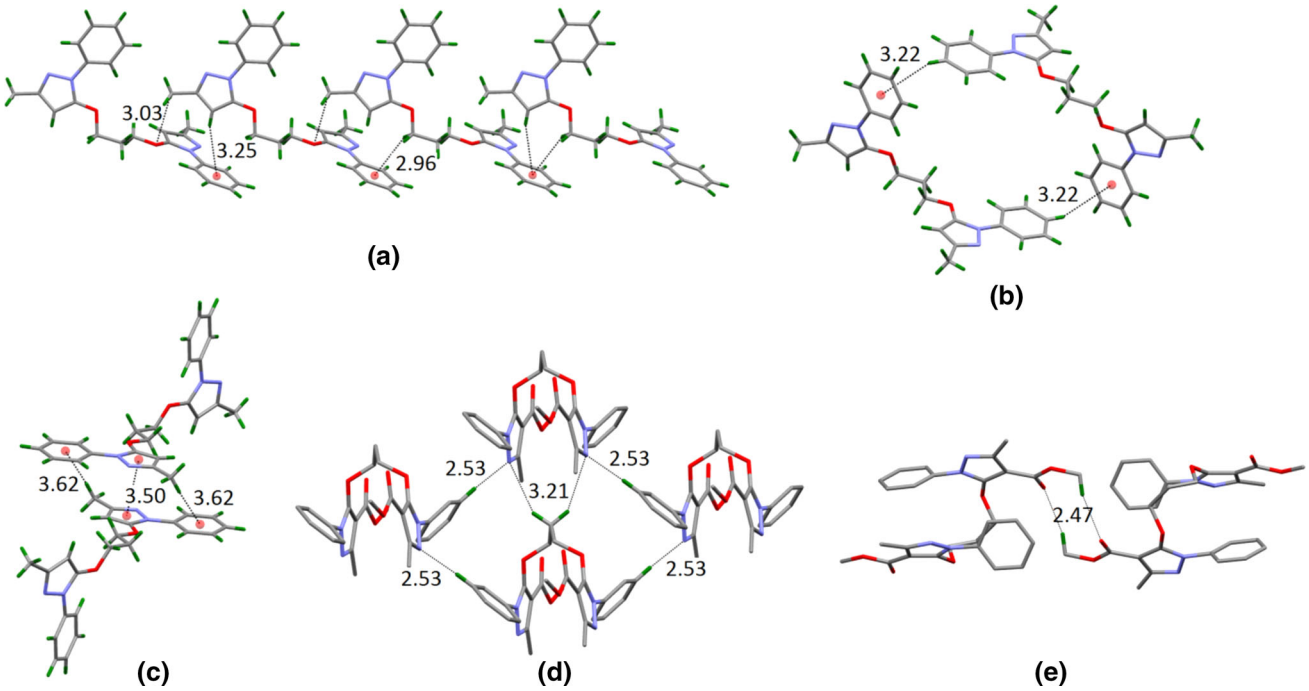

Fig. 2 **a**, **b** and **c** represent intermolecular C–H···O, C–H···π, and π···π interactions in compound **1**; **d** intermolecular C–H···N interactions forming cyclic catamer and **e** intermolecular C–H···O interaction forming dimer with $R_2^2(10)$ graph set in compound **2**. Unwanted hydrogen atoms in (**d**) and (**e**) are removed for clarity

concluded that for C–H···O, and C–H···N interactions, the D–H···A bond angle should be 90°–150°, H···A distance lies between 2.2 and 3.2 Å and D···A ranges from 3.2 to 4.0 Å between molecules [28]. Further, studies on C–H···O interactions by Desiraju added more information to the already existing data [2, 29]. Studies on C–H···π interactions show that edge-to-face orientation occurs preferentially between 2.5 and 4 Å and angle at hydrogen atom is ≥90 [30–32].

Molecular packing in the crystal structure of compound **1** was stabilized by intermolecular C–H···O, C–H···π, and π···π interactions (Fig. 2a–c). Electron deficient pyrazole ring and electron rich phenyl ring were expected to form either intermolecular π···π stack or intramolecular π···π stack. Although intermolecular π···π stacking between two pyrazole rings was stabilized by two C–H···π interactions (Fig. 2c), neither did compound 1 show intermolecular nor intramolecular reversed π···π stack. One of the pyrazole moiety in compound **1** formed an intermolecular π···π stack. The pyrazole and the phenyl rings forming the π···π stack were almost in the same plane while the other moiety was tilted at ∼25°. In contrast to the compound **1**, X-ray crystal structure of compound **2** showed intramolecular short contacts of C–H···O, C–H···N and C–H···π (Table 2) that stabilized the molecule in its folded conformation. In compound **2**, intramolecular C–H···π distance ranged from 2.90 to 3.78 Å and angles at hydrogen atom were depicted to be 86.10°, 109.65°, and 173.72°. Molecular assembly of Compound **2** indicated a tetrad formed due to strong intermolecular interactions between *meta*-hydrogen of phenyl ring of the one molecule to the 2nd nitrogen of pyrazole ring of other (Fig. 2d). This cyclic catameric network due to C–H···N interactions was responsible for generation of a symmetrical, self-assembled arrangement of molecules in space. The intermolecular C–H···O interaction between two ester groups formed a dimer of $R_2^2(10)$ graph set (Fig. 2e). The implication of an ester group in the pyrazole moiety enhanced inter as well as intramolecular interactions.

Table 2 Intramolecular H-bond geometry parameters of compound **2**

S. no.	D–H···A	H···A (Å)	D···A (Å)	D–H···A (°)
1.	C(13)–H···π (Phenyl centroid)	3.06	4.52	173.72
2.	C(6)–H···π (Pyrazole centroid)	2.90	3.34	109.65
3.	C(5)–H···π (Pyrazole centroid)	3.78	3.83	86.10
4.	C(5)–H···O(2)	3.04 (1)	3.52	112.9 (1)
5.	C(6)–H···N(2)	2.88 (2)	3.60	133.42 (9)
6.	C(13)–H···O(1)	2.47	3.01	113.17

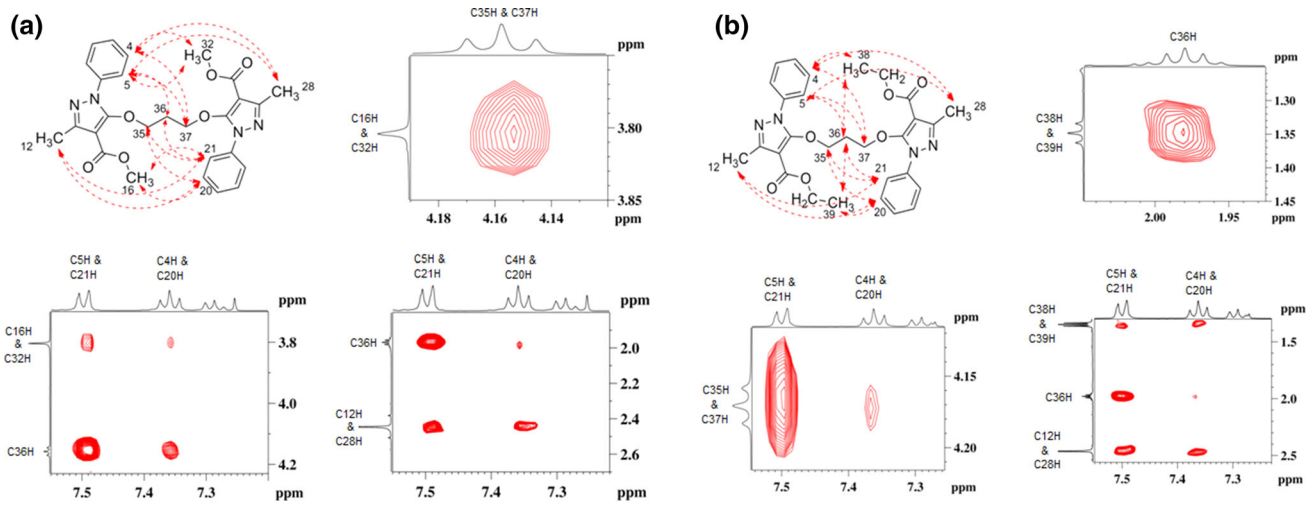

Fig. 3 Selected 2D NOE excerpts of compounds 2 (**a**) and 3 (**b**) displaying noncovalent interactions ($CDCl_3$, 400 MHz)

Since these molecules have propylene linker, it would be useful to discuss the conformation of the linker. In the solid state, compound **1** showed anti and gauche conformation between C22–C23 and C21–C22, respectively (see the numbering in ORTEP diagram in Fig. 1). Gauche conformation was stabilized by intramolecular C–H···O interaction (2.81 Å). In compound **2**, both possible conformers showed gauche conformation with C–H···O distance 2.65 Å. The detailed description of conformational stability has been discussed in computational section.

2D-NOESY experiments

2D-NOESY has been the best tool for analysing conformation based on the ^1H–^1H space interaction in solutions. Since—molecular rotations in solutions are very fast at room temperature, they may exist in several conformations, but, the equilibrium would be greater toward stable conformation. NOESY (Fig. 3) showed that compounds 2 and 3 were prevalent in folded conformation in the solution whereas compound **1** did not exist in a folded conformation because of lack of intramolecular interactions. The characteristic inter-residual NOEs interactions supported the folded conformations of compounds **2** and **3**. Presence of NOEs peaks was a direct evidence that interacting protons were below 5 Å in space [33, 34]. Selected NOEs supported reverse face-to-face stacking of compounds **2** and **3** which were (C12H & C28H) *vs.* (C4H & C20H and C5H & C21H) in both **2** and **3**, (C16H & C32H) *vs.* (C4H & C20H and C5H & C21H) in **2**, (C38H & C39H) *vs.* (C4H & C20H and C5H & C21H) in **3**. Other NOEs signals that supported the U-turn of propylene spacer was (C35H & C37H) *vs.* (C4H & C20H and C5H & C21H), (C36H) vs. (C4H & C20H and C5H & C21H) in both **2** and **3** (For detail see the supporting information Figs. S7, S8, and S9). Among the above mentioned interactions, (C12H & C28H) *vs.* (C4H & C20H and C5H & C21H) provided key evidence for reverse face-to-face stacking.

Computational studies

In order to investigate the conformational stability in gaseous state, single point energy, and optimized structure energy has been calculated at the M06-2X/6-31G (d, p) and ωB97X-D/6-31G (d, p) level of theory [35–38]. M06-2X functional was specifically developed to target nonbonding interactions and ωB97X-D contains both exchange and dispersion corrections that play important roles in correctly describing both bond changes and weak interactions. Conformations of compounds **1** and **2** have already been proposed in solids and in solution. Gaseous state optimized energy for open and folded conformation provided further idea about conformational preferences. Folded conformations of compounds **1** and **3** have been optimized by considering the same molecular frame as in compound **2**, and optimized open conformations for compounds **2** and **3** have been standardized by considering the same molecular frame as in compound **1**. The **R** group has been manipulated according to the molecule (Scheme 1). Since crystal structure of compound **3** has not been obtained therefore single point energy was calculated by considering the crystal structure of compound **2** where the methoxy group was replaced by an ethoxy group. The stabilization energies of folded conformations with respect to the open conformation obtained with ωB97X-D (M06-2X) method were 10.22 (8.23) kcal/mol, 13.93 (10.87) kcal/mol, and 14.84 (11.77) kcal/mol for compounds **1**, **2** and **3**

Table 3 Single point and optimized energy of compounds **1**, **2**, and **3**

Compound name[a]	M06-2X (kcal/mol)	ωB97X-D (kcal/mol)
1sp	−790355.11	−790433.64
1op	−790546.80	−790624.60
1fo	−790555.03	−790634.81
2sp	−1076239.83	−1076344.35
2op	−1076440.01	−1076538.87
2fo	−1076450.88	−1076552.80
3sp	−1125571.65	−1125690.21
3op	−1125761.94	−1125874.60
3fo	−1125773.72	−1125889.44

[a] ***sp*** single point, ***op*** open conformation, ***fo*** folded conformation

respectively, (Table 3; Fig. 4). Comparison of crystallographic and computed intramolecular H-bond geometry parameters for compound **2** with M06-2X and ωB97X-D functionals revealed that ωB97X-D functional was better at describing H-bond geometry parameters when compared to M06-2X. Table 4 describes the intramolecular H-bond geometry parameters of compound **1**, **2**, and **3** in folded conformation calculated with M06-2X and ωB97X-D functional. To avoid confusion and complexity in numbering, the numbering pattern for compound 2 was used as a reference while numbering compounds **1** and **3**.

This section discusses the effect of ester substituent on folding. The geometries obtained with both functionals suggest that non-covalent interaction distances viz C(13)–H···π (Phenyl centroid) and C(6)–H···π (Pyrazole centroid) are greater in compound **1** when compared to **2** and **3** while the C(5)–H···π (Pyrazole centroid) and C(6)–H···N(2) are less in compound **1** when compared to **2** and **3**. Close comparison of optimized folded conformations of compounds **1**, **2** and **3** show that presence of an ester group in **2** and **3** strengthen the stacking interactions due to the presence of C(5)–H···O(2) and C(13)–H···O(1) interactions. These interactions directly affect the C(13)–H···π (Phenyl centroid) distance which are 3.65 Å (3.67 Å) in compound **1** while 3.14 Å (3.09 Å) in compound **2** and 3.31 Å (3.36 Å) in compound **3**. Further, there is competitive interaction between C(5)–H···O(2) and C(5)–H···N(2) in compounds **2** and **3** in which C(5)–H···O(2) is dominant. Due to absence of ester group in compound **1** C(5)–H···N(2) is predominant and non-covalent interactions distance is 3.81 Å (3.88 Å). The effective interactions in folded conformation of compound **1** are C(13)–H···π, C(6)–H···π, and C(6)–H···N(2) while in compounds **2** and **3** are C(13)–H···π, C(6)–H···π, C(5)–H···O(2), C(6)–H···N(2), and C(13)–H···O(1). The C(5)–H···O(2) and C(13)–H···O(1) interactions are arisen due to implication of an ester group which is absent in compound **1**. These C–H···O distances in

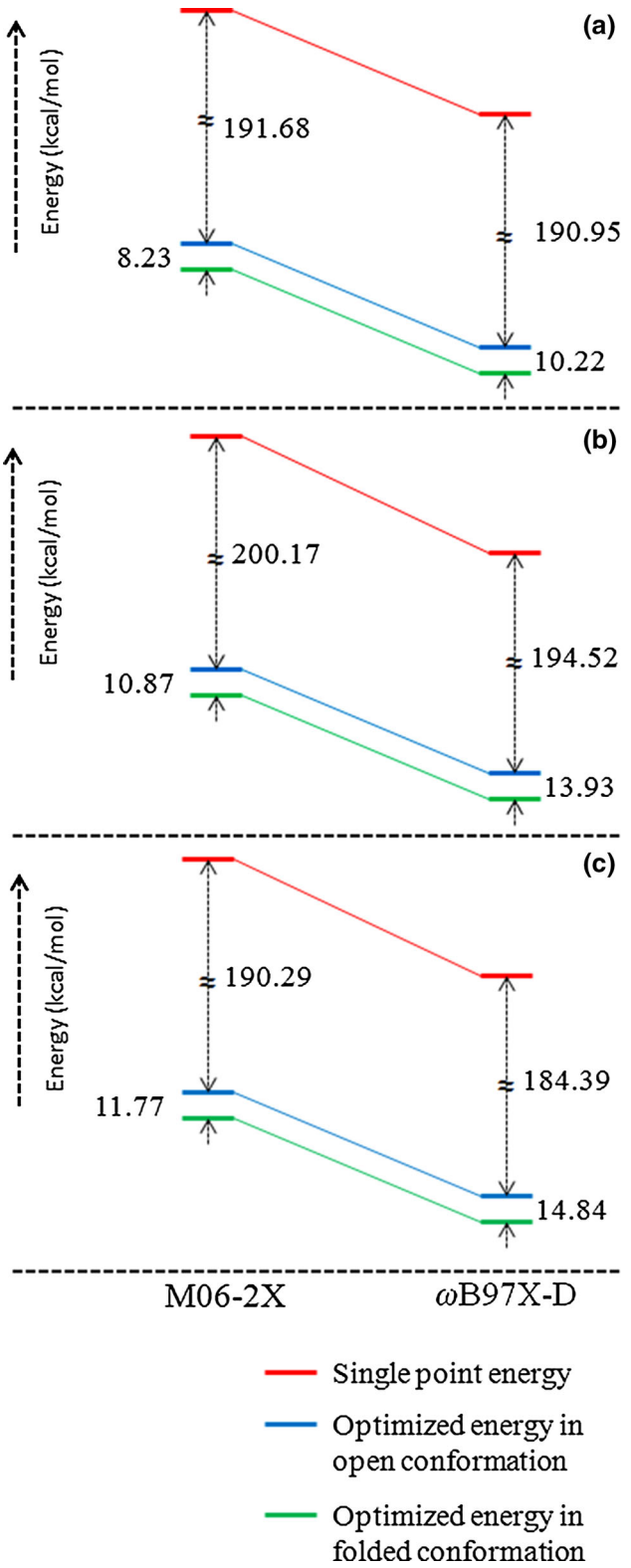

Fig. 4 Energy level diagram for single point and optimized geometry in open and folded conformation of compound **a 1**, **b 2**, and **c 3** calculated at M06-2X/6-31G (d, p) and ωB97X-D/6-31G (d, p) level of theory

Table 4 Intramolecular H-bond geometry parameters of compounds **1**, **2**, and **3** (folded conformation) calculated at M06-2X/6-31G (d, p) and ωB97X-D/6-31G (d, p) level of theory

S. no.	D–H···A	M06-2X			ωB97X-D		
		H···A (Å)	D···A (Å)	D–H···A (°)	H···A (Å)	D···A (Å)	D–H···A (°)
Compound-1							
1.	C(13)–H···π (Phenyl centroid)	3.65	4.58	161.88	3.67	4.61	146.06
2.	C(6)–H···π (Pyrazole centroid)	3.63	3.40	60.64	3.80	3.54	67.81
3.	C(5)–H···π (Pyrazole centroid)	4.16	3.73	65.95	4.26	3.82	59.77
4.	C(6)–H···N(2)	3.17	3.27	69.14	3.34	3.39	83.12
5.	C(5)–H···N(2)	3.81	3.64	72.62	3.88	3.71	72.60
Compound-2							
1.	C(13)–H···π (Phenyl centroid)	3.14	4.23	172.38	3.09	4.18	171.92
2.	C(6)–H···π (Pyrazole centroid)	3.43	3.62	90.83	3.38	3.58	91.59
3.	C(5)–H···π (Pyrazole centroid)	4.71	4.35	64.16	4.56	4.25	66.67
4.	C(5)–H···O(2)	3.07	3.16	84.36	3.14	3.27	87.17
5.	C(6)–H···N(2)	3.43	3.94	110.46	3.35	3.88	111.71
6.	C(5)–H···N(2)	5.05	4.82	71.80	4.88	4.70	74.52
7.	C(13)–H···O(1)	2.45	2.82	100.46	2.39	2.85	103.98
Compound-3							
1.	C(13)–H···π (Phenyl centroid)	3.31	4.38	166.70	3.16	4.24	169.73
2.	C(6)–H···π (Pyrazole centroid)	3.52	3.61	86.18	3.46	3.59	88.69
3.	C(5)–H···π (Pyrazole centroid)	4.83	4.38	59.34	4.62	4.27	64.50
4.	C(5)–H···O(2)	3.35	3.23	74.31	3.22	3.24	81.79
5.	C(6)–H···N(2)	3.43	3.87	105.67	3.38	3.87	108.53
6.	C(5)–H···N(2)	5.07	4.77	68.12	4.88	4.68	73.00
7.	C(13)–H···O(1)	2.42	2.83	100.54	2.41	2.88	104.09

optimized structure are close to that in crystal structure of compound **2** while other interactions (i.e. C(13)–H···π, C(6)–H···π, C(5)–H···π, C(5)–H···N(2) and C(6)–H···N(2)) are varying more. These results reveal that an ester group play key role to change the conformation from open (compound **1**) to stack (compound **2**).

Optimized structures of compounds **1**, **2,** and **3** in folded conformation are energetically stable (Fig. 5). In the folded conformation of molecules, residue O–C–C–C–O shows *gauche* conformation at propylene linker for both possible conformers and stabilize by two intramolecular C–H···O interactions. While open conformation shows one *gauche* and one *anti* conformation at propylene linker. The C–H···O distance in the *gauche* conformation is shorter in compound **1** than **3** and **3** is shorter than **2**. We observed that C–H···O distance in *gauche* conformation decreases with increasing the O–C–C–C dihedral angle. Therefore, shorter the C–H···O distance in *gauche* conformation greater would be the separation between two pyrazole moieties. Consequently, we can deduce that intramolecular contacts between two pyrazole moieties are stronger in compounds **2** and **3**.

TEM analysis

The stacked structure of compound **2** fascinated us to know its nano size crystal property. But, it is very difficult task to explain the nano-size crystal property through single crystal X-ray structure. These days TEM imaging is best tool for analyzing the property of nano structures. TEM analysis of compound **2** after 5 min from deposition of the sample on the grid showed nanoparticles with average diameter 50–70 nm (Fig. 6a). These particles are spherical or oval shape. TEM analysis within 5 min from deposition of the sample on the grid revealed that there are several spikes of almost similar size and shape, emerging out of a single core (Fig. 6b). The dimensions of the core are of between 4.05 and 21.11 nm range and the spikes are hollow in nature. The diameter of spiky arms ranges from 3.63 to 16.7 nm and the length of arms vary from 4.27 to 98.28 nm. Single crystal X-ray diffraction image manifests that intermolecular head-to-tail C–H···O interactions underpin the molecules to form channels (Fig. 6c, d). Further, these channels are forming inter-channel connections through C–H···N interactions which form the

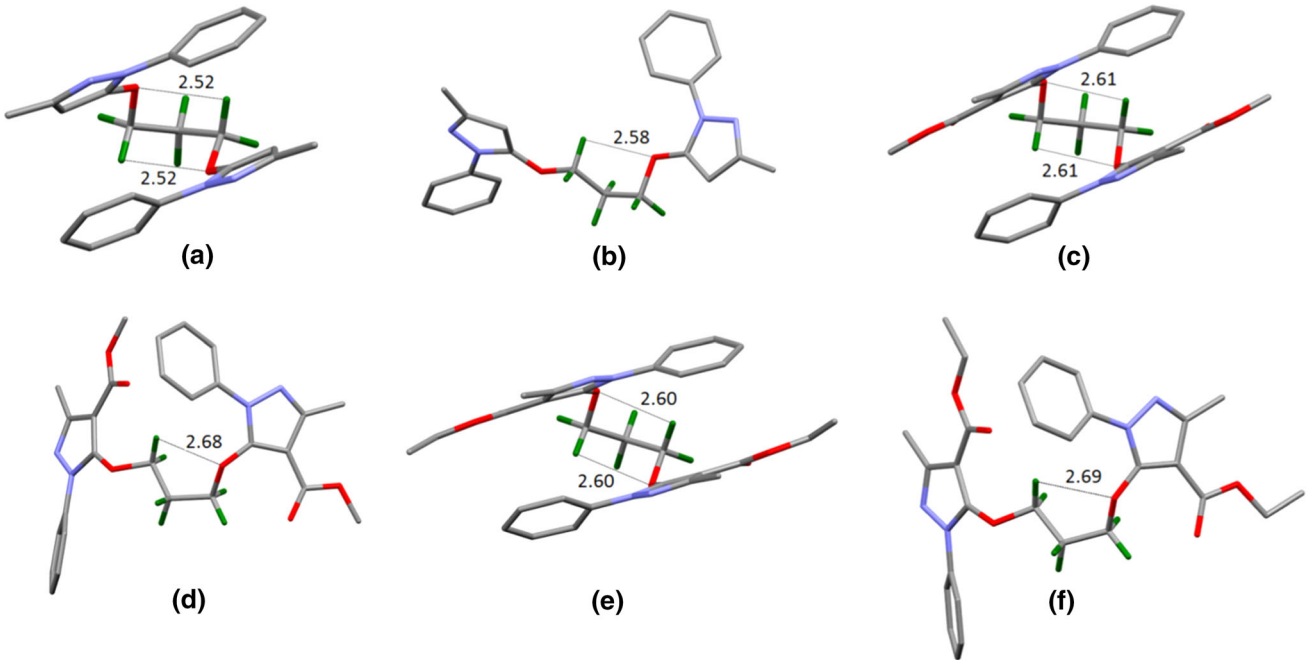

Fig. 5 Optimized structures of compounds **1** (**a**, **b**), **2** (**c**, **d**), and **3** (**e**, **f**) in open and folded conformation at ωB97X-D/6-31G (d, p) level of theory

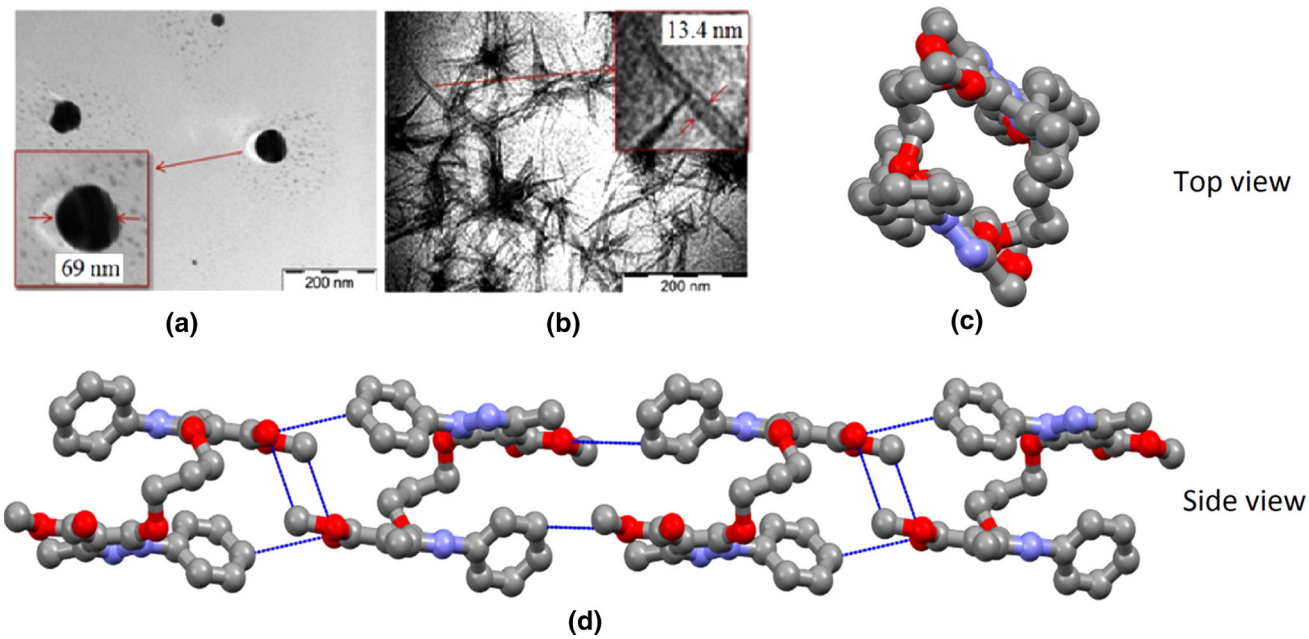

Fig. 6 TEM images of Compound **2** at 200 nm *scale* **a** showing well separated nanoparticles, **b** partially agglomerated several nanospikes although some nanospikes appeared mostly as individualized entities, **c** *top view* of the channel formed in crystal packing and **d** *side view* of the channel showing interlocking of the molecules due to the intermolecular C–H···O interactions

catameric structure (Fig. 2d) and enhance the self-assembly of channels. Consequently, agglomeration of nano spikes could be expected due to the intermolecular C–H···N interactions. Therefore, we can conclude that compound **2** has unique property to form the nano spikes with high agglomeration tendency.

Conclusions

In conclusion, we could demonstrate that single crystal X-ray diffraction analysis is the direct evidence that compound **2** shows reversed face-to-face stacking in solid state due to weak intramolecular interactions (i.e., C–H···O,

C–H···N, and C–H···π). 2D-NOESY supports that equilibrium is greater toward stacked structure for compound **2** and **3** while no evidence was obtained for compound **1** to be stacked in solution. Gaseous state stability calculated with density functional theory illustrate that folded conformation is stable for compounds **1**, **2**, and **3** while single crystal X-ray structure of compound **1** preferred the open conformation. Since, gauche or folded conformation is prevalent in a number of organic compounds [39], therefore, reverse face-to-face stacking was expected in compound **1** but it was observed in **2**. This unusual stacking was preferred due to ester group which strengthen the intramolecular interactions. The TEM image of compound **2** showed nano spikes within 5 min from the deposition of the sample on the grid with high tendency to form agglomerates which converted to nanoparticles on standing longer time than 5 min. Therefore, compound **2** showed the property of organic nanomaterials, and could draw the attention of material chemists for further study.

Acknowledgments AKT acknowledge DST India Grant no. SR/S1/OC-42/2012 for financial assistance. Department of Chemistry and Department of Anatomy (IMS), Banaras Hindu University, Varanasi, India are acknowledged for departmental facilities and TEM facility respectively. We thanks to Prof. O. N. Shrivastava Department of Physics, BHU for interpreting the TEM results. SKR also acknowledges to CSIR-New Delhi for SRF.

References

1. Hunter CA (1994) Chem Soc Rev 23:101–109
2. Desiraju GR (1995) Angew Chem Int Ed Engl 34:2311–2327
3. Hobza P, Sponer J (1999) Chem Rev 99:3247–3276
4. Jennings WB, Farrell BM, Malone JF (2001) Acc Chem Res 34:885–894
5. Brandl M, Lindauer K, Meyer M, Sühnel J (1999) Theor. Chem. Acc. 101:103–113
6. Jiang L, Lai L (2002) J Biol Chem 277:37732–37740
7. Gutfreund YM, Margalit H, Jernigan RL, Zhurkin VB (1998) J Mol Biol 277:1129–1140
8. Shivakumar K, Vidyasagar A, Naidu A, Gonnadec RG, Sureshan KM (2012) CrystEngComm 14:519–524
9. Muthuraman M, Fur YL, Beucher MB, Masse R, Nicoud JF, George S, Nangia A, Desiraju GR (2000) J Solid State Chem 152:221–228
10. Brown DT, Eisinger J, Leonard NJ (1968) J Am Chem Soc 90:7302–7323
11. Leonard NJ (1979) Acc Chem Res 12:423–429
12. Newcomb LF, Gellman SH (1994) J Am Chem Soc 116:4993–4994
13. Avasthi K, Kumar A (2012) Chem Biol Interface 2(5):258–295
14. Gellman SH (1998) Acc Chem Res 31:173–180
15. Tewari AK, Singh VP, Dubey R, Puerta C, Valerga P, Verma R (2011) Spectro Chim Acta Part A 79(5):1267–1275
16. Dubey R, Tewari AK, Ravikumar K, Sridhar B (2011) J Hetero Chem 48:691–694
17. Tewari AK, Srivastava P, Singh VP, Singh A, Goel RK, Mohan CG (2010) Chem Pharm Bull Jpn 58(5):634–638
18. Srivastava P, Singh VP, Tewari AK, Puerta C, Valerga P (2012) J Mol Struct 1007:20–25
19. Dubey R, Tewari AK, Ravikumar K, Sridhar B (2011) J Chem Crystallogr 41:886–890
20. Tewari AK, Srivastava P, Puerta C, Valerga P (2009) J Mol Struct 921:251–254
21. Avasthi K, Chandra T, Bhakuni DS (1995) Indian J Chem B34:944–949
22. Biswas G, Chandra T, Avasthi K, Maulik PR (1995) Acta Crystallogr. C51:2453–2455
23. Tewari AK, Srivastava P (2009) Synth Commun 39:2837–2842
24. Ishida T, Shibata M, Fujii K, Inoue M (1983) Biochemistry 22:3571–3581
25. Sheldrick GM (2008) Acta Cryst A A64:112–122
26. Avasthi K, Ansari A, Kant R, Maulik PR, Ravikumar K, Chattopadhyay P, Adhikary ND (2011) CrystEngComm 13:2039–2046
27. Nishio M, Umezawa Y, Honda K, Tsuboyama S, Suezawa H (2009) CrystEngComm 11:1757–1788
28. Taylor R, Kennard O (1982) J Am Chem Soc 104:5063–5070
29. Desiraju GR, Steiner T (1999) The weak hydrogen bond in structural chemistry and biology. Oxford University Press, Oxford
30. Suezawa H, Yoshida T, Hirota M, Takahashi H, Umezawa Y, Honda K, Tsuboyama S, Nishio M (2001) J Chem Soc Perkin Trans 2:2053–2058
31. Jennings WB, McCarthy NJP, Kelly P, Malone JF (2009) Org Biomol Chem 7:5156–5162
32. Sinnokrot MO, Valeev EF, Sherrill CD (2002) J Am Chem Soc 124:10887–10893
33. Gabriel GJ, Sorey S, Iverson BL (2005) J Am Chem Soc 127:2637–2640
34. Zhang R, Zeng W, Meng X, Huang J, Wu W (2012) Chem Phys 402:130–135
35. Zhao Y, Truhlar DG (2008) Acc Chem Res 41:157
36. Chai J-D, Head-Gordon M (2008) Phys Chem Chem Phys 10:6615
37. Zhao Y, Truhlar DG (2006) J Chem Theory Comput 2:1009
38. Zhao Y, Schultz NE, Truhlar DG (2006) J Chem Theory Comput 2:364
39. Takahashi O, Kohno Y, Nishio M (2010) Chem Rev 110:6049–6076